processes

MDPI

Article

Determination of Casing Wear Depth Limits for Multilateral Wells in the South China Sea

Haodong Chen [1], Aopeng Zhang [1,*], Zheng Liu [1], Xin Li [1], Zhijia Huang [1], Kai Feng [1], Rui Dai [1], Daqiu Lei [2], Liming Gao [1], Wei Zhang [1] and Haolin Song [1]

[1] Hainan Branch of CNOOC Co., Ltd., Haikou 570100, China; chenhd3@cnooc.com.cn (H.C.); liuzheng10@cnooc.com.cn (Z.L.); lixin77@cnooc.com.cn (X.L.); ex_huangzhj@cnooc.com.cn (Z.H.); fengkai5@cnooc.com.cn (K.F.); dairui2@cnooc.com.cn (R.D.); ex_gaolm2@cnooc.com.cn (L.G.); ex_zhangw22@cnooc.com.cn (W.Z.); ex_songhl@cnooc.com.cn (H.S.)
[2] CNOOC Oilfield Services Hainan Co., Ltd., Haikou 570135, China; leidq@cnooc.com.cn
* Correspondence: ex_zhangaop@cnooc.com.cn

Abstract

Casing wear is a major hidden danger affecting drilling safety and the long-term integrity of the wellbore. Excessive wear significantly reduces the casing's residual collapse strength, internal pressure, and tensile strength, and in severe cases, can lead to wellbore failure or even well control accidents. Therefore, accurately predicting casing wear is of great significance for preventing casing failure and ensuring drilling safety. Based on the wellbore structure and casing data provided on site, this study calculates casing wear using the established casing wear prediction model, and systematically analyzes the development patterns and main controlling factors of casing wear across the entire well section and under different drilling conditions. Calculation results show that within the entire well, the build-up section and the bottom casing shoe are the two areas with the most severe wear, with predicted wear depths significantly higher than those in vertical and horizontal sections. At the same time, these two regions closely match the locations where dogleg severity is pronounced in the well trajectory, indicating that dogleg severity is a key geometric factor controlling the spatial distribution of wear. This research method focuses on the correlation patterns between engineering measurable parameters and prediction results, making it easier for field engineers to understand and apply. It can provide a basis for casing residual strength evaluation, drilling parameter optimization, and drill tool combination optimization.

Keywords: casing wear; field data; wear prediction model; dogleg severity; wellbore integrity

Check for updates

Academic Editor: Tianshou Ma

Received: 9 September 2026
Revised: 25 October 2026
Accepted: 27 October 2026
Published: 9 November 2026

Copyright: © 2026 by the authors. Licensee MDPI, Basel, Switzerland. This article is an open access article distributed under the terms and conditions of the Creative Commons Attribution (CC BY) license.

1. Introduction

Casing wear has long been a critical challenge in drilling engineering. As exploration extends into deep formations, deepwater, and unconventional oil and gas fields, the drillstring experiences more severe loading and motion under complex wellbore conditions. During operations such as tripping and rotary drilling, tool joints and pipe body repeatedly rub against the inner wall of the casing, generating crescent-shaped wear grooves [1]. The reduction in wall thickness can decrease the collapse, burst, and tensile strengths of the casing, and in severe cases, may lead to wellbore collapse, leakage, or even abandonment, thereby threatening wellbore integrity and causing substantial economic losses [2]. In complex formations such as high-pressure salt-gypsum layers, brine seepage can further aggravate the deterioration of wellbore integrity [3].

Casing wear is essentially a friction-driven material removal process. Bradley and Fontenot [4] identified rotation as the primary cause through experimental studies and field sample analyses. White and Dawson [5] proposed the Casing Wear Efficiency Model (CWEM), which assumes that wear volume is proportional to side force, wear coefficient, and the number of revolutions, thereby establishing a foundation for quantitative prediction. Hall et al. [6] simplified the model and calibrated wear coefficients under various operating conditions.

As drilling environments become increasingly complex, casing wear research faces new challenges: (1) In complex-structure wells such as extended-reach horizontal wells, high dogleg severity and prolonged rotation exacerbate wear; meanwhile, wellbore stability and torque prediction issues become more prominent [7]; (2) Rotation, lateral vibration, and torsional vibration of the drillstring increase the frequency of friction and contact forces, leading to non-uniform wear [8,9]; (3) The mechanisms by which drilling fluid type, hardfacing materials, and drillstring bending strength affect wear rate remain unclear [10], and full-scale tests have shown that the wear coefficient of water-based drilling fluids is more than twice that of oil-based fluids [11]; (4) Field measurements have revealed composite wear patterns, such as overlapping, intersecting, and separated multiple crescent-shaped grooves, which go beyond the traditional single-crescent theory [12].

The accuracy of casing wear prediction directly affects wellbore integrity assessment and drilling parameter optimization. During the design stage, reasonable selection of casing grade and wall thickness can avoid overdesign or underdesign [13], while wellbore stability during the production phase and critical production pressure difference constraints should also be taken into account [14]; during the operational stage, timely prediction provides a basis for parameter adjustment and the implementation of anti-wear measures [15], while a time-dependent wellbore stability model can provide a basis for optimizing operational parameters [16]. However, current predictions still suffer from multiple uncertainties: the wear coefficient varies considerably due to differences in experimental conditions and field operations [17]; the micro-dogleg severity of wellbore trajectory is difficult to predict precisely [18]; contact force calculation is influenced by model selection [19], while a torque prediction model based on multi-source drilling data fusion can effectively improve the accuracy of contact force and torque calculations [20]; and mature theoretical models for composite wear profiles are lacking [21].

In recent years, research on casing wear has made progress in mechanisms, modeling, experiments, and mitigation measures. In terms of mechanisms, the coexistence and transition of abrasive, adhesive, and fatigue wear mechanisms have been revealed [8,22]: under dry friction and low loads, abrasive wear dominates, while under high loads and high frequencies, it shifts to adhesive and fatigue wear [22]; the influence of drilling fluids is significant, with water-based fluids causing much greater wear than oil-based fluids (which have better lubricity) [8,23], and solid particles aggravate three-body abrasion, but excessively high sand content weakens adhesive wear [4]; the addition of lubricants can effectively reduce wear.

In terms of modeling, the CWEM linear model has limitations [6]; Gao and Sun [24] introduced a variable of wear groove depth, and Guo et al. [25] incorporated the influence of wear width, both of which improved the agreement between predictions and measurements. For side force calculation, the soft-string, modified soft-string, and stiff-string models are commonly used, and can be selected in combination as needed; the stiff-string model offers higher accuracy but with greater computational cost, while the soft-string model is preferable for preliminary evaluation [1,2]. Drillstring vibration significantly increases frictional contact forces, and lateral vibration generates high dynamic loads; wear intensifies

with increasing rotational speed and weight on bit, and increases sharply when approaching critical rotational speeds [9,19].

Field measurements have revealed composite wear patterns, such as overlapping, separated, and intersecting wear grooves, which can be categorized into four types [11], and a composite wear model incorporating spatial and temporal discretization has been established [21]. Full-scale testing is an important means of obtaining wear coefficients, and the test apparatus can control load, rotational speed, and lubrication conditions, with in situ wear depth measurements showing good agreement with profilometer readings [10]. Multi-function test rigs capable of simultaneously controlling side force, rotation, reciprocation, and mud circulation have shown that the wear coefficient first reaches a peak and then decreases to a stable value, which is attributed to the reduction in contact pressure [26].

Field measurements commonly employ ultrasonic imaging tools (USIT) and multi-finger caliper logs (MFCL) [27,28]. Ultrasonic logging can estimate the wear cross-section through ellipse fitting [27]; multi-finger calipers can provide wear profiles. By combining gyroscopic surveys with offset well data to calibrate the coefficients, the prediction deviation is typically within ±2% [15]. Field management practices include recording metal weight loss, hardbanding wear conditions, and other relevant parameters, which provide a basis for early warning [2].

Prevention and control can be approached from both design and operational aspects: during the design stage, dogleg severity and side force should be controlled, while during operations, the wellbore torque should be monitored and maintained below the threshold [2]. The application of cemented carbide hardfacing and non-rotating protectors (NRP) converts steel-steel contact into polymer-steel sliding, significantly reducing the wear coefficient [29].

In summary, casing wear research has evolved from empirical understanding to a systematic stage that integrates theory, experimentation, and field applications. Nevertheless, further in-depth studies are still required regarding wear mechanisms under complex operating conditions, prediction of composite wear patterns, accurate determination of wear coefficients, and coupled analysis of drillstring dynamics and casing wear [30].

2. Casing Wear Prediction Model

In early drilling engineering research, scholars established the classic “single crescent” wear model based on laboratory experiments and field observations [5]. This model holds that under continuous contact between the drillstring and the casing, a crescent-shaped wear zone forms on the inner wall of the casing, and its geometry can be uniquely defined by two parameters: the maximum wear depth and the wear width. On this basis, White and Dawson [5] proposed a linear wear efficiency model that quantitatively relates the wear area to the rotational work performed by the drillstring. Subsequent researchers further integrated this model with drillstring force calculations, thereby developing a relatively mature technical framework of “single-crescent wear prediction and residual strength evaluation” [6].

With the large-scale development of complex oil and gas wells such as deep wells, ultra-deep wells, and extended-reach wells, the casing wear morphology is no longer the traditional single-crescent shape, but exhibits compound modes of multiple crescents overlapping, crossing, or separating. The classic single-crescent model cannot accurately describe the formation process and residual strength of such wear. To address this issue, and also considering the casing rubbing wear induced by drillstring vibration behavior in deepwater and deep-layer multi-lateral well drilling, this paper employs a drillstring rubbing–casing wear coupling model, in which the rubbing force is introduced on the basis of the conventional contact force, so as to predict casing wear under such complex working conditions.

The drillstring rubbing–casing wear coupling model adopts the following simplifying assumptions:

(1) The casing is spatially discretized along the wellbore depth into several axial elements, and the cross-section of each element is meshed along the circumferential direction;
(2) The drilling process is temporally discretized according to drilling operations and computational time steps;
(3) Wear contribution is primarily attributed to drillstring rotation and impact, while wear induced by axial friction is neglected;
(4) A linear wear efficiency model is employed, with the wear coefficient taken as constant within each time step.

These assumptions transform the complex three-dimensional wear problem into a linear accumulation process over spatiotemporally discretized elements, thereby significantly reducing the computational complexity while ensuring prediction accuracy.

Based on the above assumptions, the model is established using a dual discretization scheme in both space and time. In the spatial domain, the casing is divided into several subsections along the wellbore depth, and the cross-section of each subsection is further divided into N elements in the circumferential direction, with the vector Γ denoting the distribution of wear depth. In the temporal domain, the drilling process is discretized into elements according to drilling operations and time steps. The core of the model consists of three modules: calculation of the drillstring-casing rubbing force, calculation of the casing wear area, and updating of the wear depth [21].

First, based on drillstring dynamic analysis, the rubbing force between the drillstring and the casing is calculated considering factors such as the bottom-hole assembly, drillstring stiffness, and borehole curvature. The calculation formulas for the axial force and torque are as follows [21]:

$$\frac{\mathrm{d}F_e}{\mathrm{d}s} = -EIk\frac{\mathrm{d}k}{\mathrm{d}s} - w_{bp}t_z + \mu_d n_t(1 - kr_o cos\theta_c) + w_v \tag{1}$$

$$\frac{\mathrm{d}M_t}{\mathrm{d}s} = \mu_t r_o n_t + m_v \tag{2}$$

where F_e is the effective axial force, in N; E is the elastic modulus, in N/m^2; I is the moment of inertia, in m^4; k is the borehole curvature, in m^{-1}; w_{bp} is the buoyant weight per unit length of the pipe string, in N/m; t_z is the vertical component of the unit tangent vector of the pipe string element; μ_d is the axial friction coefficients; n_t is the distributed contact force, in N/m; r_o is the outer radius of the pipe string, in m; w_v is the dynamic viscous drag force of drilling fluid, in N/m; M_t is the torque of the drillstring; μ_t is the torsional friction coefficients; m_v is the viscous torque of drilling fluid, in N · m.

Respectively, after considering the tool joint effect. On this basis, considering the rubbing effect induced by drillstring whirl, a dynamic rubbing force component is introduced. The contact position between the drillstring and the casing is determined by the following equation [21]:

$$\theta_c = \begin{cases} \arccos\left(\frac{n_{t,n}}{n_t}\right), & n_{t,b} < 0 \\ 2\pi - \arccos\left(\frac{n_{t,n}}{n_t}\right), & n_{t,b} \geq 0 \end{cases} \tag{3}$$

Through the above model, the contact force between the drill string body, the joint, and the casing can be obtained simultaneously, n_b, n_c, and the contact position θ_c, providing mechanical input for calculating casing wear.

The solution algorithm of this module is the finite difference method: by applying the finite difference method to solve the ordinary differential equations, the differential equations are approximated as algebraic equations and then solved, thereby obtaining parameters such as the effective axial force, contact force, torque, and contact position angle

of the pipe string. Adopting the backward difference scheme, the approximate relation is given as [31]:

$$\frac{\mathrm{d}F_e}{\mathrm{d}s} \approx \frac{F_{e_i} - F_{e_{i-1}}}{\Delta s_i} \tag{4}$$

$$\frac{\mathrm{d}M_t}{\mathrm{d}s} \approx \frac{M_{t_i} - M_{t_{i-1}}}{\Delta s_i} \tag{5}$$

The nodes are numbered along increasing measured depth. The calculation proceeds from the bit toward the wellhead, i.e., in the direction of decreasing node index. The axial force and torque at the bit are prescribed as boundary conditions, and the solution is advanced node by node toward the wellhead.

Thus:

$$\frac{F_{e_i} - F_{e_{i-1}}}{\Delta s_i} + (EI)_i k_i \left(\frac{\mathrm{d}k}{\mathrm{d}s}\right)_i + w_{bpi} t_{zi} - \mu_d n_{ti}(1 - k_i r_{oi} cos\theta_{ci}) - w_{vi} = 0 \tag{6}$$

$$\frac{M_{t_i} - M_{t_{i-1}}}{\Delta s_i} - \mu_t r_{oi} n_{ti} - m_{vi} = 0 \tag{7}$$

$$cos\theta_{ci} = \frac{F_{e_i} k_i + \tau_i^2 (EI)_i k_i + w_{bpi} n_{zi} - \tau_i k_i M_{ti} + \mu_t n_{ti} sin\theta_{ci} - \tau_i \mu_d n_{ti} r_{oi} sin\theta_{ci}}{n_{ti}} \tag{8}$$

where τ is the borehole torsion, in m^{-1}.

The casing wear shape is calculated by a discretization approach: the cross-section of the casing is divided circumferentially into a number of spatial elements, and the drilling process is partitioned into a number of time elements. Within each time element, the contact position between the drillstring and the casing is determined using the torque-and-drag model, and then the wear depth of each spatial element is computed according to the wear efficiency model. The wear calculation proceeds recursively in time, with the wear profile at the current time step depending on the results from the previous time step. Finally, the wear depths of all spatial elements are accumulated to obtain the casing wear shape, which can be expressed as a wear-depth vector [11]:

$$\Gamma^j = \left[\delta_1^j \cdots \delta_i^j \cdots \delta_N^j\right]^{\mathrm{T}} \tag{9}$$

where Γ^j is the wear-depth vector of the casing segment at the end of the j-th time element; δ_i^j is the corresponding wear depth of the i-th spatial element at the end of the j-th time element, in m; and N is the number of spatial elements, which is a large even integer.

Secondly, the casing wear area within each time increment is calculated. The wear area generated per unit time increment is expressed as [21]:

$$\Delta S_b^t = 60\pi \frac{r_o}{V_f} W_f \cdot n_b^t \cdot \Delta T^t \tag{10}$$

where V_f is the rate of penetration, in m/h, W_f is the wear coefficient, n_b^t is the contact force of the t-th time micro-element, in N, i.e., the dynamic rubbing force of the drillstring, which is used as an additional component input for the wear-area calculation, and ΔT^t is the length of the time micro-element.

At the end of the j-th time element, the wear depth and the increment of wear area for each spatial element of the casing are given by [11]:

$$\Delta\delta_{ki}^j = \begin{cases} R_{ki}^j - R_{hi}^{j-1}, & R_{ki}^j > R_{hi}^{j-1} and \delta_i^{j-1} < b_0 \\ 0, & R_{ki}^j \geq R_{hi}^{j-1} and \delta_i^{j-1} = b_0 \\ b_0 - \delta_i^{j-1}, & \delta_i^{j-1} + \Delta\delta_{ki}^j \geq b_0 \end{cases} \tag{11}$$

$$\Delta S_{ki}^{j} = \begin{cases} \frac{\Delta\theta}{2}\left[\left(R_{ki}^{j}\right)^2 - \left(R_{hi}^{j-1}\right)^2\right], & R_{ki}^{j} > R_{hi}^{j-1} and \delta_i^{j-1} < b_0 \\ 0, & R_{ki}^{j} \le R_{hi}^{j-1} and \delta_i^{j-1} = b_0 \\ \frac{\Delta\theta}{2}\left[\left(R_{h0} + b_0\right)^2 - \left(R_{hi}^{j-1}\right)^2\right], & \delta_i^{j-1} + \Delta\delta_{ki}^{j} \ge b_0 \end{cases} \quad (12)$$

where $\Delta\delta_{ki}^{j}$ is the increment of wear depth, subscript k includes two cases b and c, namely drillstring body and drillstring connector, R_k is the radius of the drillstring body or connector, R_{hi}^{j} is the inner radius of casing after wear, R_{h0} is the initial inner radius of the casing before wear, and b_0 is the wall thickness of unworn casing.

First, the radial interference (Δr) is calculated based on the drillstring position and the casing inner diameter from the previous time step. If no contact occurs or the casing has already been worn through, the wear increment is set to zero. Otherwise, the wear increment is defined as the minimum of the radial interference and the remaining casing wall thickness, ensuring that the wear depth does not exceed the remaining wall thickness.

To clarify the equation provenance, Table 1 summarizes the sources and applicable conditions of the directly adopted equations.

Table 1. Sources and applicable conditions of the directly adopted equations.

Directly Adopted Equation	Applicable Conditions
Contact position angle [21]	Contact force components are known; used to determine the contact angle between the drillstring and casing; only rotary wear and linear wear efficiency are considered.
Finite difference equations [31]	Upstream or initial boundary values are known, and explicit marching; the function is required to be continuous and differentiable, the step size sufficiently small to satisfy first-order accuracy and explicit stability conditions; boundary conditions should be specified at the starting point.
Wear depth [11]	The casing is discretized axially and circumferentially, and the time domain is divided into time elements; the wear coefficient is constant at each step; only rotary wear is considered; composite wear can be described and recursively accumulated.
Wear area [11]	

Finally, based on geometric relationships, the distance between the outer edge of the drillstring and the inner wall of the casing is compared at each time step to determine the wear increment: when the drillstring exceeds the current casing profile, a wear increment is generated until the wall thickness limit is reached; otherwise, the increment is zero. Through iterative accumulation of the wear increments, the composite wear profile and depth distribution over the entire casing cross-section are ultimately obtained.

The model introduces a dynamic rubbing component, enabling it to describe composite wear patterns such as overlapping and intersecting multiple crescents. Compared with the Landmark model, which only accounts for single-crescent wear, it more accurately reflects the force conditions on the drillstring, thereby enhancing the reliability of casing wear prediction.

The friction coefficient in this composite model was calibrated using field-measured logging data. Multiple preset values of the friction coefficient were substituted into the model to calculate the corresponding surface torque variation curves, and the value that minimized the error between the calculated and measured data was selected as the optimal back-calculated friction coefficient. Based on the measured hook load and torque of Well X1 provided by the field, the friction coefficient is taken as 0.2. The wear coefficient was also calibrated by back-calculation from field-measured data. Measured casing wall-thickness reduction data were collected for the target intervals. Figure 1 compares the calculated and measured maximum wear depths of the 9-5/8-in casing in Well X2 as a function of well depth. The results show that the theoretically calculated maximum wear depth of the

casing agrees well with the measured results, and the wear coefficient obtained by inversion is $1.35 \times 10^{-12} Pa^{-1}$.

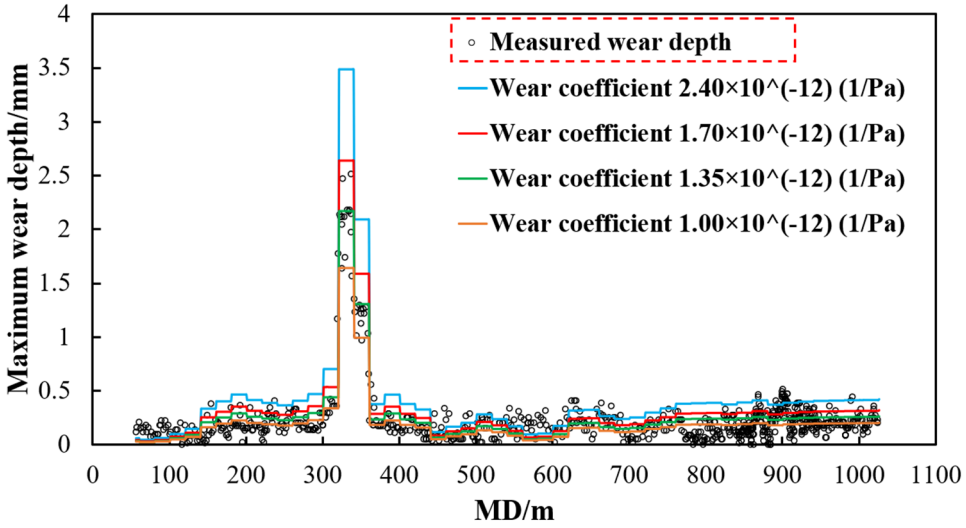


Figure 1. Measurement and prediction results of maximum casing wear depth.

The wells X1 and X2 used for validation are similar in wellbore trajectory, drilling parameters, BHA configuration, and drilling fluid properties, and they have identical casing grade and size. Therefore, the validation results are considered reasonably credible.

This composite wear model is applicable to complex intervals during rotary drilling where the wear position or drillstring outer diameter varies, producing overlapping, crossing, or separated crescents, such as deep wells, ultra-deep wells, multilateral wells, extended-reach wells, and intervals with large dogleg severity variations. It is not applicable to stages dominated by axial friction, such as tripping.

3. Geological Background and Operational Issues of the Block

In the target field, the maximum well depth exceeds 6600 m, with the longest horizontal section reaching over 2100 m, a maximum build-up rate of 3.86°/30 m, and a maximum inclination of 93°. The long horizontal wells are designed with a shallow kick-off point combined with an extra-long tangent section, which results in high contact forces between the casing and the drill string, significantly elevated drag and torque, and consequently a substantially increased risk of casing wear. As shown in Figure 2, casing wear leads to strength degradation, manifested as a decline in both burst and collapse resistance. This deterioration elevates the risks of casing deformation and leakage, thereby constraining subsequent operations.

In the wells drilled in this block, casing wear and seal failures have occurred repeatedly, manifested as abnormal annular pressure, sticking, and thread disengagement. The complex wellbore configurations result in high drag and widespread string wear; in the shallow sections, the long unsupported casing is more susceptible to failure. Meanwhile, the deep-water multilateral wells feature complex trajectories. Severe drillstring vibration adversely affects its fatigue life, and the BHA is prone to fracture. In addition, the tubing string tends to undergo buckling configuration changes under multiple operating conditions, thereby compromising operational safety.

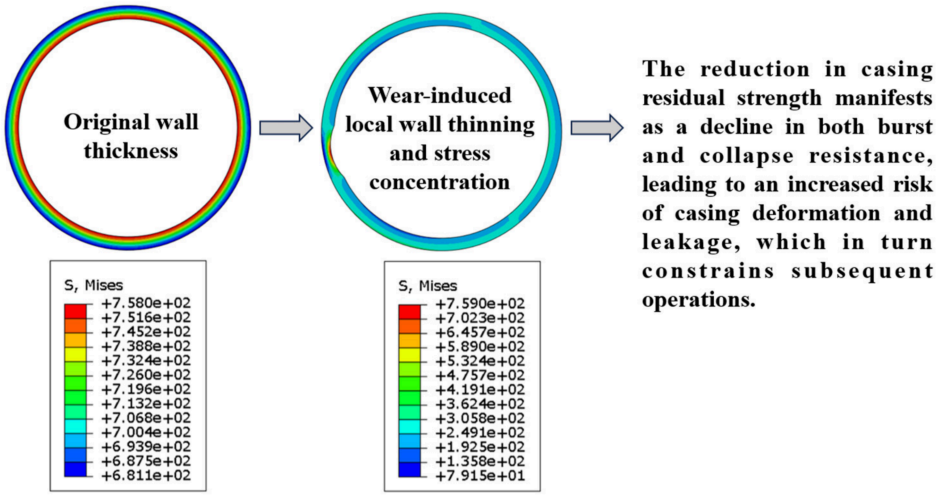


Figure 2. Schematic of casing wear hazard mechanisms.

In summary, the target block presents prominent issues including a significantly underestimated prediction of casing wear rate, unclear mechanisms of seal failure in casing connections, difficulty in accurately evaluating drillstring fatigue life, and insufficient understanding of tubing buckling behavior under multiple operating conditions. There is an urgent need to systematically investigate the contact wear mechanism between casing and drillstring, the dynamic characteristics of the drillstring, and the full-life-cycle safety evaluation of the entire string system.

Currently, in terms of string safety research and risk control for deepwater, deep-formation, multilateral, long horizontal wells, the following key issues are mainly encountered:

(1) Existing casing wear calculation methods suffer from poor adaptability and cannot accurately predict wear location, wear depth, or residual strength.
(2) Under buckled conditions, the distribution of alternating stress in the drillstring is not well understood, and its coupling with multiple sources of vibration makes fatigue life prediction difficult; the bottom-hole assembly (BHA) is complex and operating conditions are variable, leading to severe loading, and the rationality of the current BHA design and drilling parameters urgently needs evaluation and optimization.
(3) In deepwater and deep formations, tubing and screen strings are subjected to numerous operating conditions with complex variations in mechanical boundary conditions. The full-life-cycle safety evaluation methods under multiple operating conditions are not yet well-established. The coupling of temperature, pressure, and dynamic loading tends to induce string buckling and sudden state transitions, and there is a lack of targeted control measures.
(4) For the string in service, there is a lack of quantitative characterization methods for the local high stress and cascading seal failure risks induced by sudden changes in buckling state. The mechanism of sudden transitions remains unclear, and corresponding early-warning and control strategies have not yet been developed. There is an urgent need to conduct systematic research.

4. Problem Analysis

In the target block, the long horizontal wells are designed with a shallow kick-off point combined with an ultra-long tangent section, which significantly increases the contact force between the casing and the drillstring. Meanwhile, the continuous high-rate circulation further deteriorates the loading conditions of the string, resulting in generally high drag and torque in the drillstring. These engineering conditions provide a direct mechanical

driving force for the occurrence of casing wear, substantially elevating the risk of wear between the casing and the drillstring, and thus posing a severe challenge to safe drilling.

In the deepwater, deep-formation multilateral wells of this block, the well trajectories are complex. The drillstring has a long run-in-hole time and is subjected to diverse loads. During drilling, frequent collision and rubbing between the drillstring and the casing generate combined torsional and impact loads, resulting in wall-thickness reduction, strength degradation, and complex wear profiles on the casing. In the shallow sections, because the cement slurry did not return to the surface during primary cementing, the unsupported casing length is relatively long, making it more susceptible to failure. The multi-directional vibrations of the drillstring alter the contact state and force distribution, thereby affecting the wear location and morphology.

In summary, the core issues of casing wear in this block can be categorized into three aspects. First, the existing wear prediction models significantly underestimate the actual wear rate, and there is a lack of methods for accurately predicting wear location, depth, and remaining strength. Second, the evaluation techniques for seal integrity after wear are not yet mature; the mechanisms of seal failure and thread disengagement in threaded connections under coupled contact-vibration conditions remain unclear. Third, the understanding of drillstring-casing coupled dynamics is insufficient, making it difficult to reveal the spatiotemporal distribution patterns of wear from a mechanical root-cause perspective. The existence of these issues results in a lack of systematic engineering guidance for full-life-cycle casing integrity assurance. Therefore, there is an urgent need to conduct research on casing wear mechanisms and remaining strength evaluation.

5. Case Study

A case calculation is conducted for Well X3, a case well in the target block. This well is similar to Wells X1 and X2 in wellbore trajectory, drilling parameters, BHA configuration, and drilling fluid properties, and the casing grade and size are identical. The calculation results are subsequently analyzed and discussed.

5.1. Basic Information of Case Well

The wellbore configuration data of this well are presented in Figure 3, which comprises four parts: wellbore profile, east and north displacements, well trajectory data, and dogleg severity distribution, and the wellbore configuration parameters are presented in Table 2, which adopts a five-section casing program. The dogleg severity distribution is presented in Figure 3d. The designed total depth of the a main branch of Well X3 is 6264 m, with a true vertical depth of 4180 m and a horizontal section length of 1697 m; the designed total depth of the b lateral branch of Well X3 is 6369 m with a TVD of 4230 m; and the designed total depth of the c lateral branch of Well X3 is 6803 m with a TVD of 4175 m. The completed borehole size, i.e., the open hole size, for all three branches is 8-1/2 in.

Table 2. Wellbore configuration parameters of Well X3.

Well Section	Diameter (in)	Measured Depth (m)	Casing Setting Depth (m)	Casing Size (in)
Phase I	36	1458	1453	36
Phase II	26	2083	2078	20
Phase III	17-1/2	3371	3366	13-3/8
Phase IV	12-1/4	4572	4567	9-5/8
Phase V	8-1/2			Open hole section

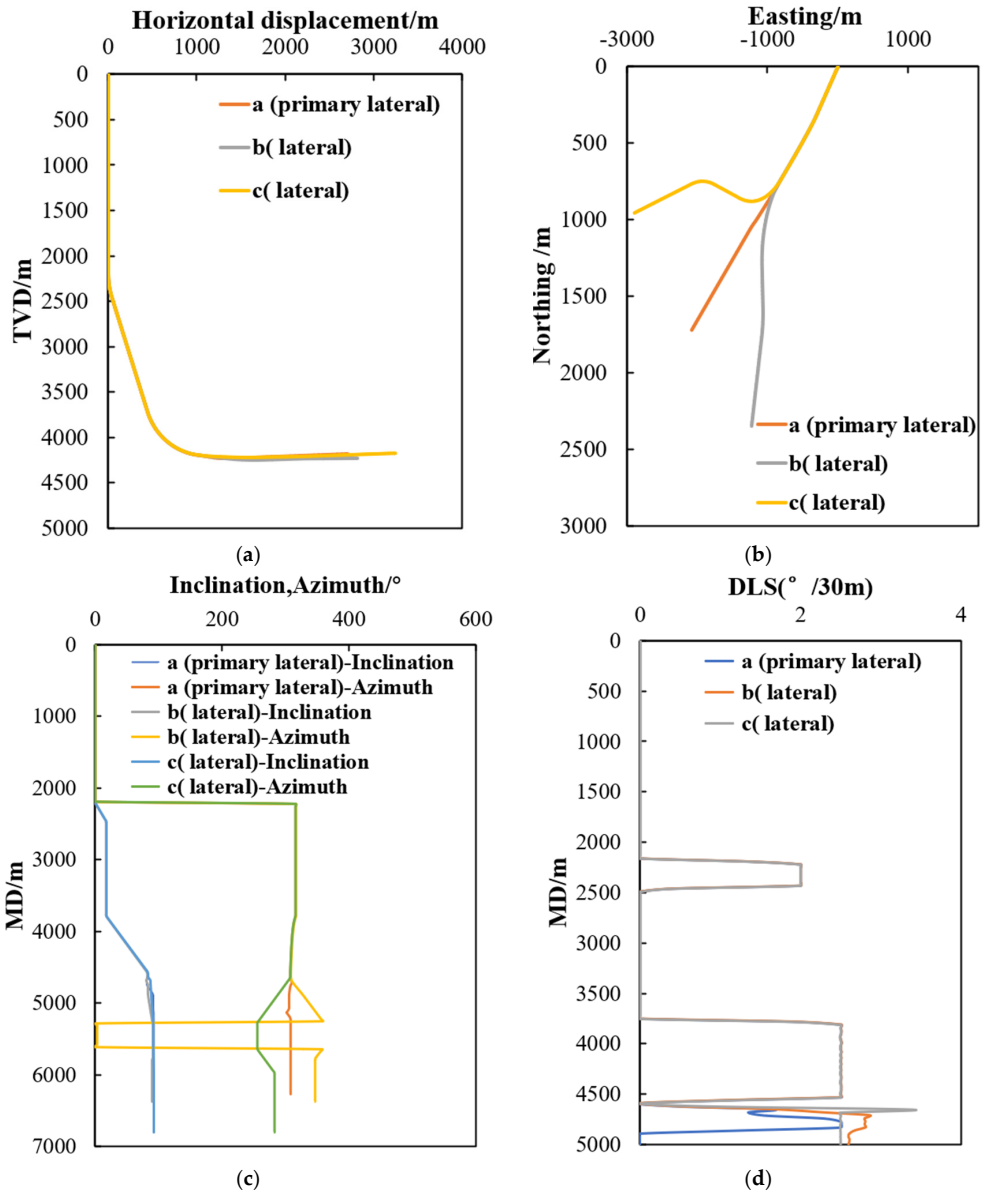


Figure 3. Wellbore configuration data of Well X3. (**a**) Wellbore profile; (**b**) East displacement vs. North displacement; (**c**) Well trajectory data plot; (**d**) Dogleg severity distribution.

Table 3 lists the basic input parameters required for the wear prediction model and residual strength calculation used in this study. The detailed drill string assembly configuration, including the inner diameter, outer diameter, tool joint outer diameter, yield strength, and length of each drill pipe section, is summarized in Table 4.

Table 3. Basic Parameters for Wear Prediction and Residual Strength Calculation.

Casing Grade	Casing OD	Casing Wall Thickness	Mud Density	Number of Axial Grid Elements	Number of Circumferential Grid Elements	WOB	Rotary Speed
P110	9-5/8 in	13.8 mm	1200 kg/m^3	10	360	100 kN	100 rpm

Table 4. Drillstring configuration and input parameters used in the wear calculation.

Item	Pipe ID (mm)	Pipe OD (mm)	Tool Joint OD (mm)	Yield Strength (MPa)	Length (m)
Drillpipe 1	71.37	171.45	190.50	725	12.50
Drillpipe 2	50.80	171.45	190.50	725	49.56
Drillpipe 3	77.80	127.00	165.10	725	131.60
Drillpipe 4	108.60	127.00	168.30	724	2000.00
Drillpipe 5	130.90	145.57	177.80	724	4071.34

5.2. Analysis of Wear Prediction Results

This subsection presents the analysis of the wear prediction results for the 9-5/8-in casing in Well X3, which mainly comprises two parts: the analysis of the calculated maximum casing wear depth and the analysis of casing coupling wear.

(1) Analysis of predicted maximum casing wear depth

Based on the calculations from the casing wear prediction model, the casing wear conditions of the three branches of Well X3 are analyzed. Figure 4 presents the distribution of the maximum casing wear depth along the entire wellbore for each of the three branches of Well X3 after their respective completion.

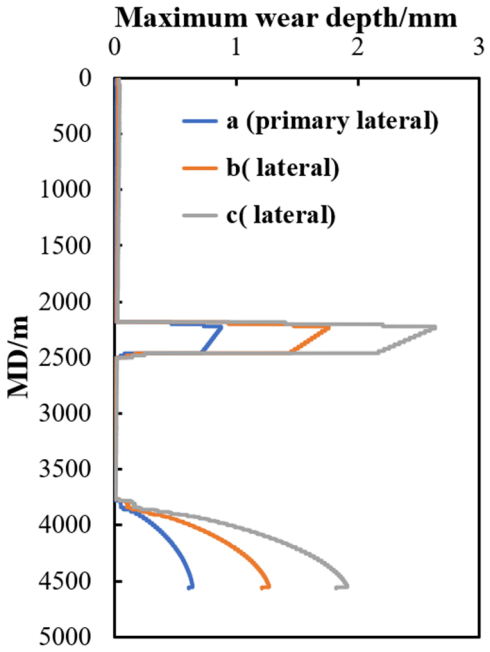


Figure 4. Maximum casing wear depth over the entire wellbore section.

The results indicate that, with increasing well depth, the maximum casing wear depth generally exhibits a relatively gentle fluctuation with small magnitude at shallow depths, then increases sharply near the kick-off point of Well X3 and rapidly decreases back to the previous gentle range, and finally shows a gradual increase near the casing shoe at the bottom. The calculated maximum wear depths are 0.88 mm for the a main branch, 1.76 mm for the b lateral branch, and 2.64 mm for the c lateral branch. The maximum wear depth occurs at a depth of 2221 m, which is the first kick-off point of this well. After the completion of the three branches, the maximum wear depth at the first kick-off point is 19.1%, and the maximum wear degree at the casing shoe is 13.9%. In addition, at positions where the wellbore trajectory has higher dogleg severity, the casing wear is relatively large.

According to the wear mechanism analysis, the severe wear at the kick-off point is mainly attributed to the large wellbore curvature, which causes a sharp increase in the side force and contact force of the drillstring; meanwhile, the variation in the force direction of the drillstring leads to superposition of wear tracks, forming compound wear, with local damage accumulation being the most prominent. The increase in wear near the casing shoe is due to the severe vibration and whirl of the bottom hole assembly in the open hole section, which produces repeated impact and scraping against the casing shoe; in addition, the structural discontinuity at the casing shoe induces contact stress concentration, further accelerating local wear.

Selected cross-sectional wear profiles of the casing at representative intervals are used to analyze the casing wear shape, as shown in Figure 5. For Well X3, the intervals selected are the first kick-off point and the bottom casing shoe location. In the figure, the cross-sectional shape of the casing is depicted using polar coordinate plots with the outer and inner radii of the casing; the numbers on the outer circle denote the angular coordinate values (°) in polar coordinates, and the numbers along the radial direction denote the radial coordinate values (mm). The description of the morphological features primarily exhibited by the wear at 2221 m and 4500 m shown in Figure 5 is intended to illustrate the model's ability to predict other wear patterns that may occur under complex operating conditions, and does not represent the measured geometry of this well.

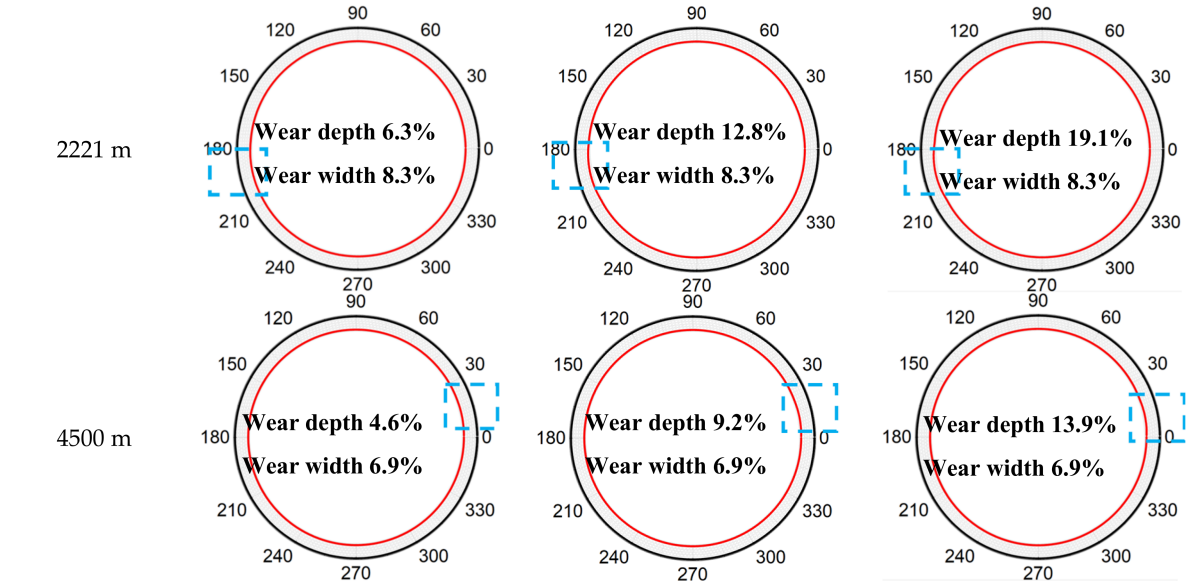


Figure 5. Sections at the first kickoff point and casing shoe locations.

After the completion of the a main branch of Well X3, selected cross-sectional wear profiles at two representative intervals are used to analyze the casing wear shape, as shown in Figure 5a. The results indicate that at the first kick-off point (2221 m), the casing exhibits a single wear scar with a wear position of approximately 192°, a wear width ranging from 177° to 207° (8.3%), and a maximum wear depth of 0.88 mm (6.3%), presenting a crescent-shaped overlapping wear pattern. Near the casing shoe location (4500 m), there is also a single wear scar with a wear position of approximately 22°, a wear width ranging from 358° to 22° (6.9%), and a maximum wear depth of 0.64 mm (4.6%), also exhibiting a crescent-shaped overlapping wear pattern.

After the completion of the b lateral branch of Well X3, selected cross-sectional wear profiles at two representative intervals are used to analyze the casing wear shape, as shown in Figure 5b. The results indicate that at the first kick-off point (2221 m), the casing exhibits

a single wear scar with a wear position of approximately 192°, a wear width ranging from 177° to 207° (8.3%), and a maximum wear depth of 1.76 mm (12.8%), presenting a crescent-shaped overlapping wear pattern. Near the casing shoe location (4500 m), there is also a single wear scar with a wear position of approximately 22°, a wear width ranging from 358° to 22° (6.9%), and a maximum wear depth of 1.27 mm (9.2%), also exhibiting a crescent-shaped overlapping wear pattern.

After the completion of the c lateral branch of Well X3, selected cross-sectional wear profiles at two representative intervals are used to analyze the casing wear shape, as shown in Figure 5c. The results indicate that at the first kick-off point (2221 m), the casing exhibits a single wear scar with a wear position of approximately 192°, a wear width ranging from 177° to 207° (8.3%), and a maximum wear depth of 2.64 mm (19.1%), presenting a crescent-shaped overlapping wear pattern. Near the casing shoe location (4500 m), there is also a single wear scar with a wear position of approximately 22°, a wear width ranging from 358° to 22° (6.9%), and a maximum wear depth of 1.91 mm (13.9%), also exhibiting a crescent-shaped overlapping wear pattern.

Overlapping crescent wear is caused by variations in the drillstring outer diameter at the same wear location. For example, the drillstring body and tool joints may wear the casing at the same position, or drillstring sections with different outer diameters may wear the casing at the same position.

(2) Determination of casing wear boundary

Following the casing string strength design procedure for well X3, the internal and external pressure profiles are computed for the most critical loading scenario. The load profile obtained under this scenario is then compared with the residual strength curve, and the intersection point of the two curves defines the critical residual strength. By integrating this critical value with the established mapping relationship between residual strength and wear depth, the casing wear limit is inversely determined. This method evaluates collapse and burst separately as independent failure modes, with the deterministic worst-case load case as the governing condition, without considering their coupling. Similarly, the present study calculates the residual collapse and burst strengths independently to determine the wear limit.

The residual strength assessment in this study is conducted using a two-dimensional finite element numerical simulation. The main model input parameters (including material properties, loading conditions, and failure criteria) are listed in Table 5.

Table 5. Key finite element model inputs for residual strength assessment.

Element Type	Loading Conditions	Boundary Conditions	Failure Criterion (Burst)	Failure Criterion (Collapse)
2D plane strain element	Uniform internal or external pressure applied	No displacement constraints	Equivalent stress at the mid-wall of the main wear area reaches the yield strength	Ovality of the casing cross-section reaches the critical value (0.05)

Figure 6 presents a comparison of the calculated internal and external pressure profiles with the corresponding residual burst and collapse strength curves, respectively. The results indicate that an intersection exists between the external pressure profile and the residual collapse strength curve. The residual strength at this intersection defines the critical value, which is determined as 47.7 MPa (a reduction of 36.4% from the original strength). Accordingly, the derived casing wear limit (i.e., wear depth) is 2.2057 mm, corresponding to 16% of the nominal wall thickness.

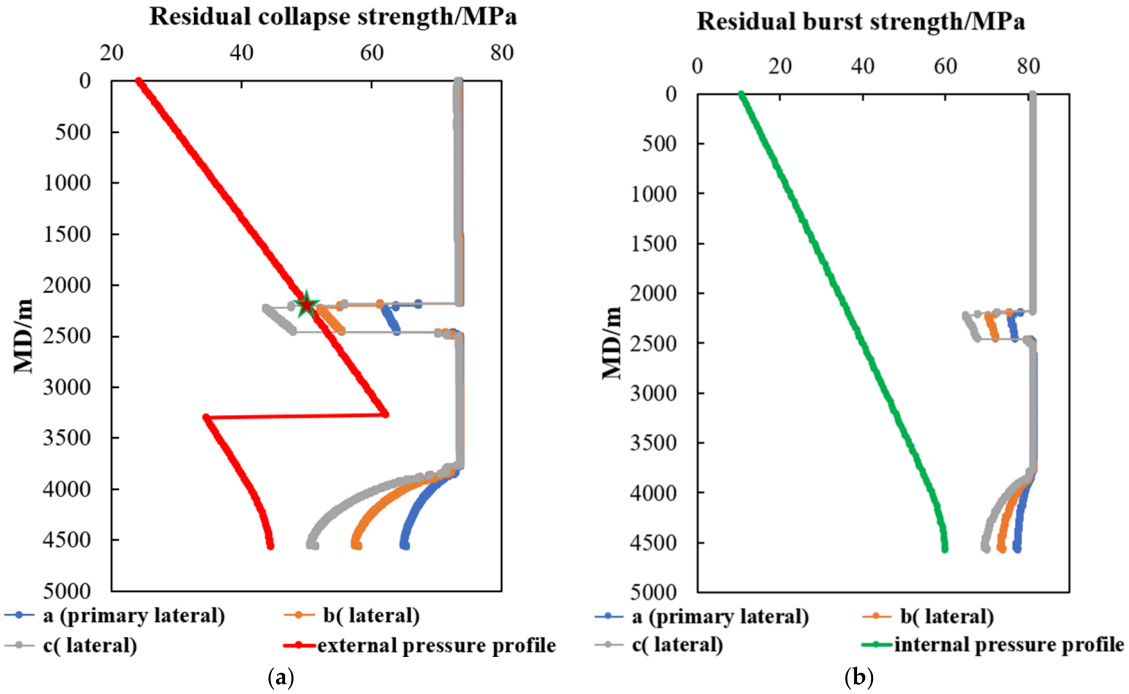


Figure 6. Determination of the critical residual strength. (**a**) Residual collapse strength; (**b**) Residual burst strength.

After determining the wear limit, the assumptions and limitations of the residual strength assessment should be clarified. In this study, temperature, axial load, bending, ovality, manufacturing tolerance, corrosion, cement support, formation pressure uncertainty, and transient differential pressure are not considered, whereas eccentric wear is incorporated by importing the wear profile into the finite element model. These unconsidered factors will constrain the applicability of the 16% wear limit obtained in this study.

6. Conclusions

(1) Based on the casing wear prediction model, a back-calculation of the friction coefficient and the wear coefficient is performed. The measured hook load and torque data from Well X1, together with the measured wear data of the 9-5/8-in casing from Well X2, are compared with the calculated results of the prediction model. The results show that with a friction coefficient of 0.2 and a wear coefficient of 1.35×10^{-12} Pa^{-1}, the predicted wear depth agrees well with the measured data, confirming the applicability of the model.

(2) During the subsequent drilling of lateral branches in a deep multilateral horizontal well, based on the model prediction results, the casing wear exhibits a significant cumulative superposition effect. The severely worn zones are predominantly characterized by overlapping crescent-shaped wear scars. This phenomenon is attributed to the periodic variation in the outer diameter of the drillstring passing through the same wellbore section—specifically, when the drillpipe body and the tool joints (or components with different outer diameters) successively traverse the same interval, the differences in contact load and contact area produce multiple eccentric and misaligned crescent-shaped wear scars on the inner wall of the casing. After repeated superimposition, these scars eventually form an asymmetric and irregular wear profile.

(3) The calculation results indicate that the maximum wear depth of the 9-5/8-in casing is pronounced at both the first kickoff point and the bottom casing shoe of Well X3, and the dogleg severity at these two corresponding locations is relatively high, suggesting a

close correlation between the wear severity and the borehole curvature. Therefore, the casing at the first kickoff point and the casing shoe is subject to a higher risk of wear, and these positions should be prioritized as key foci for residual strength evaluation and optimization of anti-wear measures.

(4) Through calculation and back-calculation, this study focuses on the cumulative wear at the first kickoff point (2221 m) and near the casing shoe location (4500 m) for the three branches of Well X3, and proposes a 16% wall-thickness wear limit for this block. Under the model adopted in this paper and the specific load conditions, when the wear depth actually predicted or measured for this well exceeds this threshold, it indicates a potential operational risk.

Author Contributions: H.C.: Conceptualization, Validation, Resources, Writing—original draft. A.Z.: Conceptualization, Supervision, Writing—review & editing. Z.L., X.L. and Z.H.: Conceptualization, Supervision, Writing—review & editing. R.D., K.F., D.L., L.G., W.Z. and H.S.: Methodology, Validation. All authors have read and agreed to the published version of the manuscript.

Funding: The authors gratefully acknowledge the financial support from the CNOOC through its Comprehensive Scientific Research Program (Grant No. KJZH-2025-2302), with the project title "Research on Key Technologies for Safe and Efficient Drilling and Completion in Deepwater and Deep-buried Strata in the South China Sea."

Data Availability Statement: The data presented in this study are available from the corresponding author upon reasonable request and with the approval of the project client. The data are not publicly available due to confidentiality/proprietary restrictions.

Conflicts of Interest: Authors Haodong Chen, Aopeng Zhang, Zheng Liu, Xin Li, Zhijia Huang, Kai Feng, Rui Dai, Liming Gao, Wei Zhang and Haolin Song were employed by the company Hainan Branch of CNOOC Co., Ltd. Author Daqiu Lei was employed by the company CNOOC Oilfield Services Hainan Co., Ltd. The authors declare that the research was conducted in the absence of any commercial or financial relationships that could be construed as a potential conflict of interest. The funder was not involved in the study design, collection, analysis, interpretation of data, the writing of this article or the decision to submit it for publication.

References

1. Cao, T.B.; Li, Z.H.; Liu, J.; Meng, F.Q.; Zhang, W.C. Casing Wear Prediction and Residual Strength Calculation for Extended-Reach Wells. *Sci. Technol. Eng.* **2024**, *24*, 10227–10234.
2. Liu, Y.; French, P.; Skinner, G.; Gleizes, L.; Bisset, P.; Gajare, S.; Kelleher, D.; Razzetto, M. Integrated Casing Wear Management in Well Design and Drilling Operations with a Field Case Analysis. In Proceedings of the SPE Asia Pacific Oil & Gas Conference and Exhibition (APOGCE), Perth, Australia, 15–17 October 2024.
3. Li, B.; Liu, N.; Zhu, M.; Chen, X. Numerical Study on the Influence of Saltwater Seepage in High-Pressure Salt-Gypsum Layers on Wellbore Integrity. *J. Compos. Sci.* **2025**, *9*, 160. [CrossRef]
4. Bradley, W.B.; Fontenot, J.E. The Prediction and Control of Casing Wear. *J. Pet. Technol.* **1975**, *27*, 233–245. [CrossRef]
5. White, J.P.; Dawson, R. Casing Wear: Laboratory Measurements and Field Predictions. *SPE Drill. Eng.* **1987**, *2*, 56–62. [CrossRef]
6. Hall, R.W.; Garkasi, A.; Deskins, G.; Vozniak, J. Recent Advances in Casing Wear Technology. In Proceedings of the IADC/SPE Drilling Conference, Dallas, TX, USA, 15–18 February 1994.
7. Hao, Z.; Huang, P.; Tan, Z.; Yang, F.; Feng, L.; Chen, X. Wellbore Stability for Extended-Reach Drilling in Deep Coal Seams Under Heterogeneous In Situ Stresses: A Laboratory-Calibrated Framework. *Processes* **2026**, *14*, 62. [CrossRef]
8. Osman, O.A.; Merah, N.; Abdul Samad, M.; Baig, M.M.A.; Samuel, R.; Alshalan, M.; Alshaarawi, A. Casing Wear and Wear Factors: New Experimental Study and Analysis. *Materials* **2022**, *15*, 6544. [CrossRef] [PubMed]
9. Liu, J.L.; Wan, Z.G.; Man, Z.F.; Li, G.P.; Xia, X.; Luo, J.B.; Dou, Y.H. Analysis of Irregular Casing Wear Morphology Induced by Rubbing. *Pet. Mach.* **2024**, *52*, 56–61.
10. Osman, O.A.; Merah, N.; Samuel, R.; Alshalan, M.; Alshaarawi, A. Casing Wear Tests for Precise Wear Factor Evaluation. In Proceedings of the IADC/SPE International Drilling Conference and Exhibition, Galveston, TX, USA, 8–10 March 2022.
11. Zhang, X.; Huang, W.; Gao, D. Prediction Model of Casing Wear Shape and Residual Strength under Compound Modes. *SPE J.* **2022**, *27*, 2183–2203. [CrossRef]

12. Mitchell, S.; Xiang, Y. Improving Casing Wear Prediction and Mitigation Using a Statistically Based Model. In Proceedings of the IADC/SPE Drilling Conference and Exhibition, San Diego, CA, USA, 6–8 March 2012.
13. Carpenter, C. Study Investigates Casing Wear in the Culzean Field. *J. Pet. Technol.* **2023**, *75*, 73–75. [CrossRef]
14. Ge, J.; Li, G.; Li, Y.; Cai, B.; Chen, X.; Yang, J.; Chen, T.; Zeng, J. A New Predictive Model for Open-Hole Wellbore Stability During the Production Phase of Ultra-Deep Extended-Reach Wells Based on Critical Production Pressure Difference Constraints. *Processes* **2025**, *13*, 3373. [CrossRef]
15. Aichinger, F.; Dao, N.H.; Brillaud, L.; Nobbs, B.; Delapierre, A.; Pinault, C.; Rossi, X. Systematic Field Validation of New Casing Wear Quantification Process. In Proceedings of the Abu Dhabi International Petroleum Exhibition & Conference, Abu Dhabi, United Arab Emirates, 7–10 November 2016.
16. Wei, Q.; Chen, T.W.; Xing, X.S.; Yan, X.J.; Zhou, C.S.; Chen, X.Y.; Zeng, J.; Yang, Y.Y.; Yang, Q.Q. A time-dependent wellbore stability model considering rheology-damage coupling for offshore shallow mudstone extended-reach drilling. *Results Eng.* **2026**, *32*, 112672. [CrossRef]
17. Aichinger, F.; Brillaud, L.; Nobbs, B.; Couliou, F.; Oyovwevotu, J.; Mathieson, G.; Vavasseur, D.; Hardie, J. Casing Wear: Prediction, Monitoring, Analysis and Management in the Culzean Field. In Proceedings of the SPE Annual Technical Conference and Exhibition, Dubai, United Arab Emirates, 21–23 September 2021.
18. Mertens, R.; Vecseri, J.; Kotara, B.; Spreafico, D. Casing Wear Modeling and Mitigation of a Sidetrack on a Challenging Deepwater Well. In Proceedings of the Offshore Technology Conference, Houston, TX, USA, 5–8 May 2025.
19. Samuel, R.; Kumar, A. Modeling Method to Estimate the Casing Wear Caused by Vibrational Impacts of the Drillstring. In Proceedings of the IADC/SPE Drilling Conference and Exhibition, Fort Worth, TX, USA, 4–6 March 2014.
20. Ge, J.; Li, P.; Liu, W.; Cai, B.; Li, Y.; Chen, X.; Yuan, X.; Tang, P. Construction of an Extended-Reach Well Torque Prediction Model Based on Multi-Source Drilling Data Fusion and Analysis of Dominant Factors. *Processes* **2026**, *14*, 2801. [CrossRef]
21. Huang, W.J.; Zhang, X.K.; Gao, D.L.; Shi, X.L.; Su, P. A Computational Model for Predicting Casing Wear Profile and Depth under Combined Wear Modes. *Pet. Res.* **2021**, *42*, 1373–1381.
22. Gouveia, L.P.; Ferro, A.P.A.; Ferreira, D.V.G.; Junior, E.T.L.; Barboza, A.S.R.; Percy, J.G.; Riente, A.F. Casing Wear Log Using a Prewear Ellipse Shape from Ultrasonic Logging Data. *SPE J.* **2022**, *27*, 2642–2654. [CrossRef]
23. Mencaglia, X.; Cazier, O.; Feutry, V.; Almeida, G.; Brillaud, L. Towards a Novel Approach to Consider Casing Wear in Well Designs. In Proceedings of the Offshore Technology Conference, Houston, TX, USA, 2–5 May 2022.
24. Gao, D.; Sun, L. New Method for Predicting Casing Wear in Horizontal Drilling. *Pet. Sci. Technol.* **2012**, *30*, 883–892. [CrossRef]
25. Guo, K.Y.; Cui, G.; Sun, L.; Yu, H.T.; Wang, Y.R. Prediction and Analysis of Casing Wear in Complex Structure Wells. *Neijiang Sci. Technol.* **2024**, *45*, 76–77.
26. Yaqoob, T.; Oppelt, J.; Holzmann, J.; Schamp, J. Localized Wear in Steel, Glass Fiber and Composite Casings Upon Drillstring Contact: A Full-Scale Experimental Comparison. In Proceedings of the Offshore Technology Conference Asia, Kuala Lumpur, Malaysia, 27 February–1 March 2024.
27. Zhang, Q.; Lian, Z.; Lin, T.; Deng, Z.; Xu, D.; Gan, Q. Casing Wear Analysis Helps Verify the Feasibility of Gas Drilling in Directional Wells. *J. Nat. Gas Sci. Eng.* **2016**, *35*, 291–298. [CrossRef]
28. Patel, H.; Baldino, S.; Ozbayoglu, E.M. Enhanced Casing Wear Assessment: A New Experimental Approach to Wear Factor Evaluation with Insights into Flow Regimes, Tool-Joint Materials, and Presence of Cuttings. *SPE J.* **2025**, *30*, 4561–4576. [CrossRef]
29. Dou, Y.H.; Zhang, F.X.; Wang, W.J.; Zhang, S.L. Analysis of Casing Wear Depth and Residual Strength in Downhole Environments. *Oil Drill. Prod. Technol.* **2007**, *29*, 36–39.
30. Yang, Q.Q.; Chen, X.Y.; Li, G.C.; Huang, P.; Chao, Z.X.; Li, P.B.; Zhang, Z.L. Numerical analysis of wellbore stability based on thermal-fluid-solid coupling in deep well drilling. In Proceedings of the 59th U.S. Rock Mechanics/Geomechanics Symposium, Santa Fe, NM, USA, 8–11 June 2025. [CrossRef]
31. Sun, L.Z. *Study on Prediction and Control Method of Friction and Wear of Pipe String in Complex Structure Wells*; University of Petroleum (Beijing): Beijing, China, 2012.

Disclaimer/Publisher's Note: The statements, opinions and data contained in all publications are solely those of the individual author(s) and contributor(s) and not of MDPI and/or the editor(s). MDPI and/or the editor(s) disclaim responsibility for any injury to people or property resulting from any ideas, methods, instructions or products referred to in the content.